

Interference Microscopy Volume Illustration for Biomedical Data

Hanqi Guo^{1,2} Xiaoru Yuan^{1,2 *} Jie Liu^{1 †} Guihua Shan³ Xuebin Chi^{3 ‡} Fei Sun^{4 §}

- 1) Key Laboratory of Machine Perception (Ministry of Education), and School of EECS, Peking University
- 2) Center for Computational Science and Engineering, Peking University
- 3) Computer Network Information Center, Chinese Academy of Sciences
- 4) Institute of Biophysics, Chinese Academy of Sciences

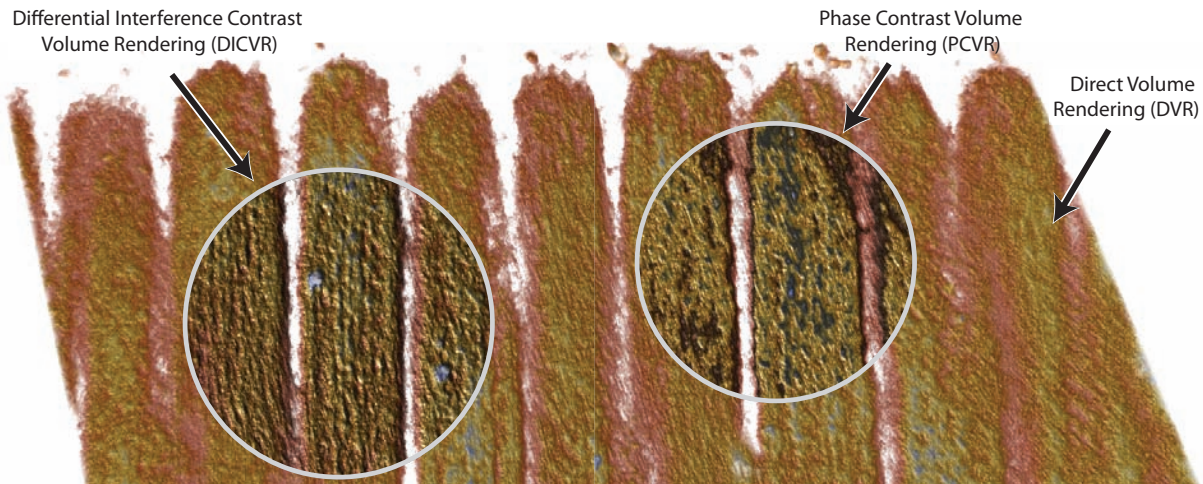


Figure 1: Visualization results of a mouse intestine microvilli data set with lens of DICVR (Differential Interference Contrast Volume Rendering) and PCVR (Phase-Contrast Volume Rendering) in the context of DVR (Direct Volume Rendering). While both methods can enhance the structure details of the noisy data, DICVR is able to clearly depict the small micro-filament structures in each microvillus.

ABSTRACT

In this paper, we propose a novel volume illustration technique inspired by interference microscopy, which has been successfully used in biological, medical and material science over decades. Our approach simulates the optical phenomenon in interference microscopy that accounts light interference over transparent specimens, in order to generate contrast enhanced and illustrative volume visualization results. Specifically, we propose PCVR (Phase-Contrast Volume Rendering) and DICVR (Differential Interference Contrast Volume Rendering) corresponding to Phase-Contrast microscopy and Differential Interference Contrast (DIC) microscopy respectively. Without complex transfer function design, our proposed method can enhance the image contrast and structure details according to the subtle change of Optical Path Differences (OPD), and illustrate the thickness change and occluded structures with interferometry metaphors. In addition, we also develop a user interface to enable slicing specimen sections in volume data. Focus+context lens are also included in the system for convenient data navigation and exploration. As the proposed methods are based upon widely applied microscopy techniques, they are intuitive for domain experts to explore and analyze the volume data with the proposed methods. The feedbacks from domain users suggest our proposed techniques are useful volume visualization approaches complementary to the traditional ones.

*e-mail: {hanqi.guo,xiaoru.yuan}@pku.edu.cn

†e-mail: liujianju@gmail.com. Now at Content Tech, NVidia Corporation, participated in this work during his internship at Peking University.

‡e-mail: {sgh,chi}@sccas.cn

§e-mail: feisun@ibp.ac.cn

Keywords: Volume illustration, volume rendering, interference microscopy, biomedical visualization, feature enhancement.

Index Terms: I.3.3 [Computer Graphics]: Picture/Image Generation—; I.3.8 [Computer Graphics]: Applications—;

1 INTRODUCTION

One of the major challenges in volume visualization is how to effectively present sophisticated structures in the data. Direct Volume Rendering (DVR), which is a well-developed technique widely used in many applications from medical diagnosis to scientific research and engineering, is capable of depicting the appearance and the shape of the 3D volumetric data. However, the straightforward approaches are not always the most effective way to convey important features in different data. For example, achieving good DVR results relies much on data quality and Transfer Function (TF) design [16]. It is very difficult to generate high quality DVR images if the data is noisy or hard to be classified by TFs.

Recently, visualization researchers have begun to learn from traditional imagery techniques that are developed long before the computer era. For example, in history, technical illustrations effectively depict information by omitting or simplifying unimportant details while enhancing the most significant features. In modern visualization techniques, illustration techniques have also been introduced to the volume visualization domain [8]. Photographic techniques have also been investigated by visualization researchers for applications in volume illustrations, such as schlieren [27] and interferometry experimental based methods [2] used in flow visualization.

In this paper, we propose Phase Contrast Volume Rendering (PCVR) and Difference Interference Contrast Volume Rendering (DICVR), inspired from interference microscopy practice. Microscopy is the technical field of using microscopes to view small specimens. Optical and electron microscopy involve the reflection, diffraction, refraction of light and other electromagnetic radiation

incidents, and the subsequent collection of the scattered radiation to reconstruct an image. Since its invention over four centuries ago, microscopy has undergone tremendous improvement for better depiction of subjects. Phase-contrast microscopy, developed by the Dutch physicist Frits Zernike in the 1930s, is a widely used technique that can convert differences in refractive index as differences in contrast. Based on phase-contrast microscopy, Nomarski further invented Differential Interference Contrast (DIC) microscopy to enhance the contrast in transparent and unstained specimens. The volume visualization techniques we have developed in this paper simulate the above wave interference based microscopy approaches.

The general principle of light interference is that the coherent wavefronts from light cancel or reinforce each other according to the differential travel paths they traverse prior to their superposition. In the visualization model of PCVR and DICVR, Optical Path Differences (OPD) defined by the integration of the paths of the viewing rays traversing the volumetric object to be visualized. These path differences then modulate the lighting intensity to generate the interference patterns, which are similar to the enhanced effects that could be observed with phase-contrast and DIC microscopy. In Fig. 1, an example of interference inspired volume illustration is demonstrated. The proposed methods help on enhancing the contrast and emphasizing boundary regions inside the volume data, without complex TF design. We can interactively visualize volumetric data by leveraging commodity graphics hardware. Our method is simple, easy to implement and effective at illustrating subtle but critical volumetric features. Although some strip-like artifacts may be imported in the image, but they can illustrate the variations in the structures. The proposed methods also generate comparable images with real microscopy images, which are familiar to domain users.

The remainder of the paper is organized as follows. We briefly discuss related work in Section 2 followed by an introduction to the interference phenomena in Section 3. Then we describe PCVR and DICVR thoroughly in Section 4 and Section 5 respectively. The user interface design is presented in Section 6, followed by results in Section 7. The feedback from domain scientists in Section 8. Finally we conclude our work in Section 9.

2 RELATED WORK

Enhancing features in volumetric data visualization is an area of active research. The quality of a volume visualization result depends on whether the technique emphasizes important features, subjugates non-critical information and deemphasize distraction as possible.

TFs [16], which convert the voxel data values to optical properties thus hide redundant data and highlight important features, are one of the most important parameters in direct volume rendering. TF design can be categorized as data-centric and image-based methods [20]. Image-based TFs are goal oriented, while data-centric TFs focus on the numerical properties of the volume data. For example, The classification and visual effects of rendered image can be enhanced by accounting derivative properties and leveraging multidimensional transfer functions [13, 14]. However, TF design is still very difficult for non-expert users.

Ebert and Rheingans introduced the concept of volume illustration [8] by modulating each voxel’s color and opacity according to the local and global properties of the volume model. Perception of structure, shape, orientation, and depth relationships in a volume model are enhanced by the combination of direct volume rendering with non-photorealistic rendering techniques. Boundaries are enhanced by opacity modification based on the gradient value. Oriented features such as silhouettes are enhanced by calculating the dot product of the viewing direction and value gradient of the volume. The opacities of volume features oriented toward the viewers are decreased to emphasize feature orientation. Depth-cueing is

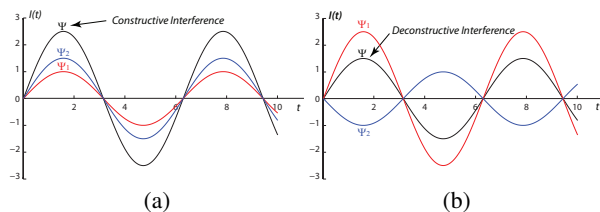


Figure 2: The illustration of light interference. Red and blue curves are two coherent waves respectively, and the black curve is the interference results. (a) constructive interference; (b) destructive interference.

achieved by shifting color according to the distance between each volume sampling point and the viewer. Svakhine et al. [26] further created a flexible illustration system incorporating domain knowledge of illustration styles to generate images with an appearance similar to medical illustrations.

Various NPR styles have been generated, such as pen-and-ink style [28, 7], halo effects [25, 4] and stippling [18, 17]. Interrante enhanced transparent surface shape and position with sparse textured ridge and valley lines [12]. Csébfalvi [5] visualized the volume contours based on the magnitude of local gradient information and the angle between viewing direction and gradient vector. Yuan and Chen [29] illustrated surface features in a volume by combining direct volume rendering with image based iso-surface silhouette/contour detection and rendering. Halos around features were introduced to reinforce the perception of depth relationship with the scene [8, 25]. Later a GPU-based volumetric halo rendering method was proposed by Bruckner and Gröller [4]. Halos are defined through TFs to classify structures of interest based on data value, direction and position. Luft et al. [19] enhanced the perceptual quality of images that contain depth information by a method similar to an unsharp mask. Motivated by artwork, the difference between the original depth buffer content from the rendering and a low-pass filtered image copy was utilized to determine information about spatially important areas and undergo local enhancement on the contrast, color, and other parameters of the image. Svakhine et al. [27] combined schlieren and shadowgraphy with silhouettes to reduce visual clutters of oriented structural information.

There are also developments focused on simulating interference effects [6, 10, 24]. Our work is not intended to fully simulate the interference phenomena, but to provide new volume visualization approaches with corresponding counterparts in microscopy domain and for visualizing volume structures and features.

3 LIGHT INTERFERENCE AND LIGHT REFRACTION

Light interference, which is one of the most common physical phenomenon in daily life, has been applied in many scientific and engineering practice, including measurement and precise control, hologram, experimental flow visualization, etc. The physics of interference has been studied for more than 300 years. Formally, Interference is the interaction of two or more waves passing the same point. Waves can enhance or cancel out each other depends on their difference of phases or paths length, a.k.a OPD. Constructive interference (Fig. 2(a)) occurs when the waves add in phase, producing a larger peak than either wave alone, whereas destructive interference (Fig. 2(b)) occurs when waves add out of phase, producing smaller peaks than one of the waves alone. Two waves with same amplitudes but exact reversed phases could totally cancel out each other.

Consider the interference of two coherent monochromatic waves with different amplitudes and initial phases:

$$\psi_n(\mathbf{x}, t) = \sqrt{I_n} \cos(2\pi ft + \phi_n(\mathbf{x})), \quad (1)$$

where $I(\mathbf{x})$ is irradiance, f is the frequency and $\phi_n(\mathbf{x})$ is the phase at position \mathbf{x} , $n = 1, 2$. Since they have the same frequency f , the irradiance of the combined wave is:

$$I(\mathbf{x}) = |\psi|^2(\mathbf{x}) = I_1 + I_2 + 2\sqrt{I_1 I_2} \cos \delta(\mathbf{x}), \quad (2)$$

where

$$\delta(\mathbf{x}) = \phi_1(\mathbf{x}) - \phi_2(\mathbf{x}) = \frac{2\pi d(\mathbf{x})}{\lambda}, \quad (3)$$

$\delta(\mathbf{x})$ is the phase difference arising from path length difference if the initial phases are the same, and $d(\mathbf{x})$ is the OPD at \mathbf{x} . If $I_1 = I_2 = I_0$ then

$$I = I_0(1 + \cos \delta(\mathbf{x})) = 2I_0 \cos^2 \frac{\delta(\mathbf{x})}{2} = 2I_0 \cos^2 \frac{\pi d(\mathbf{x})}{\lambda}. \quad (4)$$

Constructive interference occurs when the phase difference between the two waves is an even integer multiple of π . Destructive interference occurs when the phase difference between the two waves is an odd integer multiple of π . The properties of wave interference are elegantly applied in phase-contrast microscopy to enhance images of almost transparent objects.

In optical media, due to the refraction of the light, the wave length λ will be changed. Optical path (denoted as Δ) is defined as the geometry length multiples the refraction rate n . In varying refraction rate media, optical path along a ray is defined as the integral form:

$$\Delta = \int_L n(\mathbf{x}) ds, \quad (5)$$

where $n(\mathbf{x})$ is the refraction rate at position \mathbf{x} , so the OPD of the two rays can be defined as the difference of optical paths:

$$d = \Delta_2 - \Delta_1 = \int_{L_2} n(\mathbf{x}) ds - \int_{L_1} n(\mathbf{x}) ds. \quad (6)$$

Based on the observation and practice on interference and refraction phenomenon, biologists and optical physicists began to invent new microscopy technologies to visualize the transparent specimens that are not easy to be observed with traditional brightfield or darkfield microscopy. Such specimens are hard to be dyed, or living cells will go bad after staining. Although the transparent materials do not affect colors of light, but the light path and phase are changed after the light traverses through the specimen. New generation of microscopy is invented to visualize the unseen specimens with light interference, such as phase contrast microscopy and differential interference contrast microscopy. In following sections, the detailed principles and configurations of the both microscopy technologies will be described.

4 PHASE-CONTRAST MICROSCOPY AND PHASE-CONTRAST VOLUME RENDERING

Phase-contrast microscopy was a revolution of optical technique in history. It enhances the contrast obtained by the optical microscopies. Transparent specimens, such as living cells in culture, microorganism, thin tissue slices and fibers, which are almost invisible with regular microscopy without dyeing, can be easily observed with the phase-contrast technique. By simulating the optical train of phase-contrast microscopy, similar visual effects can be visualized for volumetric data.

4.1 Phase-Contrast Microscopy

A modern phase-contrast microscope is illustrated in Fig. 3(a), together with a schematic illustration of the phase-contrast optical train. The tungsten-halogen lamp produces partially coherent light. The illumination is then directed through a collector lens and focused on a specialized annulus (labeled as condenser annulus) positioned in the substage condenser front focal plane. Light wavefronts passing through the annulus illuminate the specimen. Part of the light passes through undeviated (denoted as D-wave) and another part (denoted as S-wave) are diffracted and retarded in phase

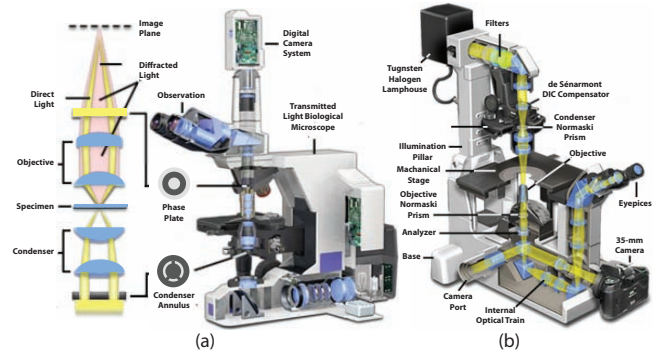


Figure 3: The configuration of interference microscopes: (a) Phase-contrast microscope; (b) Transmitted and inverted de Sénarmont Differential Interference Contrast (DIC) Microscope. Image courtesy from Nikon MicroscopyU, <http://www.microscopyu.com>

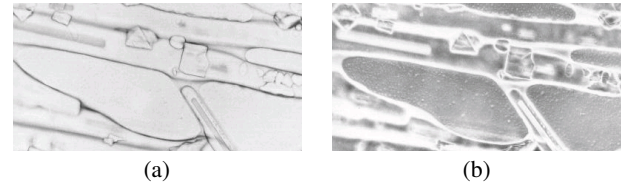


Figure 4: Phase-contrast microscope image: (a) microscopy image of crystals of strontium chloride with standard bright-field; (b) image obtained by phase-contrast microscopy. Image courtesy from Microscopy Primer (<http://www.microscopy-uk.org.uk/primer/special.htm>).

due to structures and phase gradients present in the specimen. Undeviated and diffracted light collected by the objective is segregated at the rear focal plane by a phase plate and then focused at the intermediate image plane to form the final phase-contrast image which is observed in the eyepieces. Since the undeviated and diffracted light have different phases, the final intensity of the light can be computed by equation 2 if the absorption effect is neglected. In general, the amplitudes of the undeviated and diffracted light are not the same.

Fig. 4 illustrates two images with normal brightfield microscopy and phase-contrast microscopy respectively. The specimen being examined is crystals of strontium chloride. With the phase-contrast, the details of the crystal surfaces are enhanced.

4.2 Phase-Contrast Volume Rendering

We apply the above phase-contrast enhancement to visualize structures in volume. We develop our visualization method by imitating the way interference that is applied in phase-contrast microscopy. In our visualization pipeline (Fig. 5), OPDs are defined by the integration of the density values along the viewing ray path of the volume data. The DVR image is generated by standard raycasting method, along with the data classification with transfer functions. The optical path length These path differences then modulate the lighting intensity to generate the interference patterns and enhance the contrast.

The simplified physical model for PCVR is illustrated in Fig. 6(a). Like most volume rendering techniques, PCVR and DICVR are also based upon physical model of light transport. In general, on each point in volume data, there are three types of light interactions taken into account, including emission, absorption, and scattering. The most commonly used optical model is called emission-absorption model [9]. PCVR further accounts the optical path length and phase of the rays during the ray casting pass based on the emission-absorption model.

The PCVR pipeline consists of several major steps. As illus-

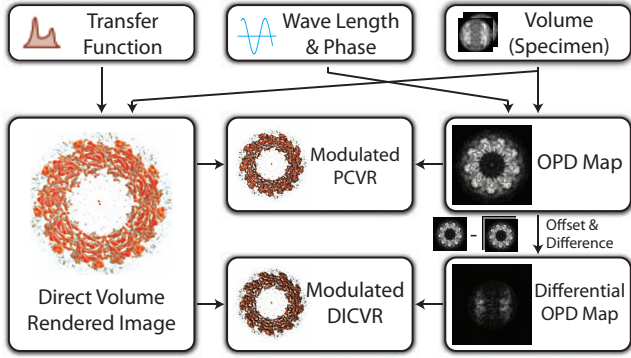


Figure 5: The pipeline of interference microscopy volume illustration. The OPD map and differential OPD map can be generated with GPU-based raycasting. The PCVR and DICVR results are achieved by modulating DVR images with OPD map and differential OPD map respectively.

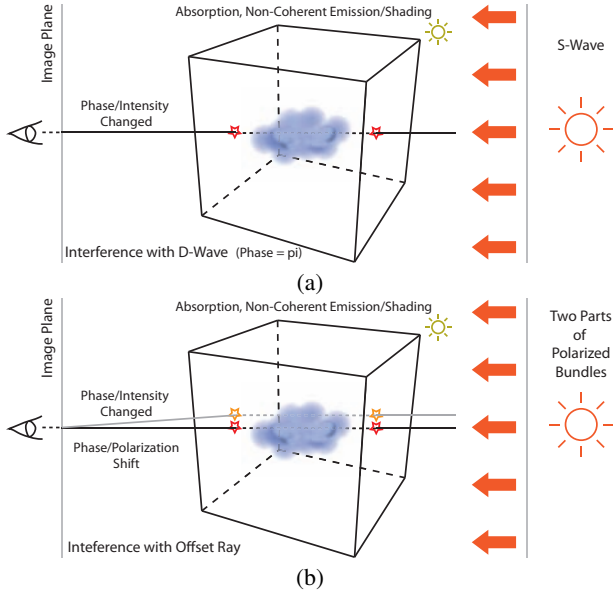


Figure 6: The simplified physical model for phase-contrast microscopy in PCVR (a) and DICVR (b).

trated in Fig. 5, the OPD image and DVR image can be first computed from volume data by volume ray casting on the GPU individually. Then the PCVR image is obtained by modulating DVR image and transformed optical path length image according to Eq. 4.

4.2.1 Optical Path Difference Computation

As described above, OPDs are defined by the integration of the density values along the viewing ray direction. Here we make an analogy between the density of the volume and the refractive index. For each sample point in the volume, the refractive index is n . Following the definition of optical path (Eq. 5), the optical path Δ in volume rendering is defined as

$$\Delta = \int_{t_0}^{t_1} n(s) ds. \quad (7)$$

Since the refractive index n is always greater than the index in vacuum 1, for convenience, we can define the index of refraction as

$$n(s) = 1 + D(s), \quad (8)$$

where $D(s)$ is the volume density value at location s . Alternatively, the index of refraction can also be defined as a mapping f from density value:

$$n(s) = 1 + f(D(s)), \quad (9)$$

where the mapping f can be defined by users, or a linear mapping by default. Part of the volume can be removed by setting $f(D(s))$ of particular volume range. It is similar to the common TF design for regular volume rendering (TF for refractive index). On the other hand, the optical path of the S-wave which passes through the volume is

$$\Delta_S = \int_{t_0}^{t_1} 1 + f(D(s)) ds, \quad (10)$$

where t_0 and t_1 are the in and out position of the ray on the volume box. The optical path of D-wave is

$$\Delta_D = \int_{t_0}^{t_1} 1 ds. \quad (11)$$

In this way, the OPD d of the S-wave and the D-wave can be computed as:

$$d = \Delta_S - \Delta_D = \int_{t_0}^{t_1} f(D(s)) ds. \quad (12)$$

The OPD can be effectively calculated by raycasting, which accumulates $f(D(s))$ from the eye position towards the volume. When each ray passes through the volumetric object, an integration computation is performed instead of volume composition in regular direct volume rendering. To achieve the interactivity, we resort to GPU for acceleration [15, 21, 22]. Specifically, we utilize a modified approach similar to what Kruger and Westermann have proposed [15] for OPD computation. After the integration, each ray returns a floating number. We effectively generate a high dynamic range image through above computation. Interference or phase-contrast computation can then be applied on the above image to obtain the enhanced image with interference patterns. Notice that the ray should not be early terminated as standard DVR often applies for acceleration. If the ray is terminated early, the OPD of the rest part will not be integrated.

4.2.2 Interference Computation

After the calculation of OPD through volume ray casting, the light intensity due to the interference effect in the phase-contrast process can be computed by a cosine function, which can be effectively evaluated in modern computer graphics hardware. The cosine function could also be substituted by other periodic function for more volume illustration effects. The most important parameter being defined in this stage is the frequency f . In general, we design the value of f to make the range of integrated OPD around $1/4\lambda$ of wavelength of the virtual interference light. The approach is widely used in the phase-contrast microscopy applications. A higher frequency number can be applied to enhance the local details.

4.2.3 Modulation with Direct Volume Rendering

The image generated from the above phase-contrast computation has only one amplitude component, which can further modulate with DVR images for final result. The modulation is applied per pixel in the rendered image space after the OPD d is obtained:

$$I' = 2\mu \cos^2 \frac{\pi d}{\lambda} + (1 - \mu)I, \quad (13)$$

where I and I' are the original and modulated luminance of the pixel, and μ is the modulation factor, which is defined by users. If $\mu = 1$, which means full modulation, then Eq. 13 is

$$I' = 2 \cos^2 \frac{\pi d}{\lambda}. \quad (14)$$

5 DIC MICROSCOPY AND DIC VOLUME RENDERING

DIC microscopy is another type of interference microscopy technique, which can enhance the contrast in transparent and unstained specimens. Compared to phase-contrast, microscopy utilizes the differential of OPDs to enhance features, instead of direct interference with OPD. DIC can help users analyzing the structures of specimens, because it is more sensitive to variation than phase-contrast microscopy.

5.1 DIC Microscopy

As shown in Fig. 3(b), the configuration of a DIC Microscope is much more complicated than phase-contrast microscopy. In addition to interferometry, DIC also exploits polarization of lights to enhance the contrast of the image. In the optical train, the semi-coherent bundles of non-polarized white light from the lamp filament is divided into two orthogonally polarized parts, which are mutually coherent. One of the two parts is slightly sheared at the sample plane, so that there are small a OPD between the two parts after they penetrated the specimens. After further optical processing, the two coherent parts are recomposited into one image. The phase offset of the two parts can also be adjusted by users.

The image quality of DIC is often better than phase-contrast images when used in suitable occasions. DIC can emphasize the contrast of lines and edges, since the contrast is approximately proportional to the gradient of OPD. It also brings strong stereoscopic sensation and emboss effects. Although the image of DIC microscopy is not topographically accurate image, DIC can play as an analytical method for sensitive measurement of the optical properties of the specimen.

5.2 DIC Volume Rendering

Like PCVR procedure, we simulate the light train of DIC microscopy in order to enhance the contrast of the features in direct volume rendering. Since the pipeline (Fig. 5) and the simplified physical model of DICVR (Fig. 6(b)) is close to PCVR, we only briefly present and introduce the different components of DICVR. There are three major steps in DICVR, including OPD map generation, differential OPD map generation, and the modulation with DVR. All the steps are performed on GPU, as described in Section 4.2.

In DICVR, differential OPD map is defined as the neighborhood pixel difference of OPD map, which can be formularized as:

$$d = \int_{t_0}^{t_1} 1 + f(D(s))ds - \int_{t'_0}^{t'_1} 1 + f(D(s))ds, \quad (15)$$

where t_0, t_1 are the entrance and exit point of the ray, and t'_0, t'_1 are the corresponding points of the offset ray, which passes through the surrounding medium. Since the offset is very tiny, we can simply assume that

$$t_1 - t_0 \approx t'_1 - t'_0. \quad (16)$$

Then the differential OPD map can be defined as

$$d \approx \int_{t_0}^{t_1} f(D(s))ds - \int_{t'_0}^{t'_1} f(D(s))ds. \quad (17)$$

On GPU implementation, the differential OPD map can be obtained by adding a offset pass and difference pass after the generation of the OPD map (Fig. 5). The interference computation and DVR modulation process is almost identical to the corresponding steps in PCVR. Notice that the wave length and phase can also be adjusted in DICVR for fine tuning.

6 USER INTERFACE DESIGN

In this section, we briefly describe several featured components in the user interface.

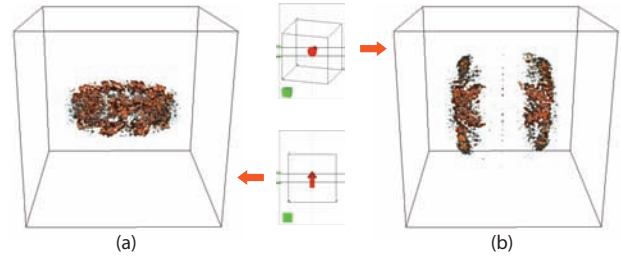


Figure 7: Linked view of the specimen slicer

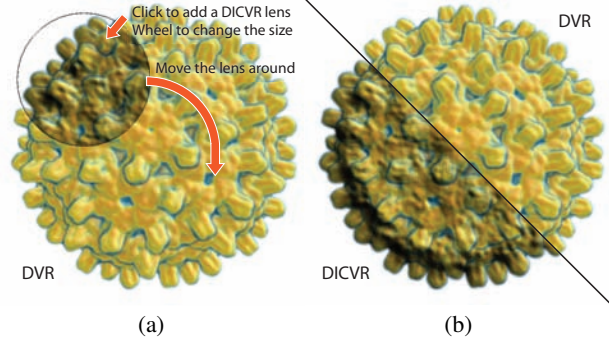


Figure 8: The visualization result of Hepatitis B Virus (HBV) [1] Cryo-EM data with focus+context lenses.

6.1 Specimen Slicer

As we described above, both phase-contrast and DIC microscopy are not good at viewing specimens that are too thick. Biologists are accustomed to examining thin slices as the sample of the object, which are fixed at the object stage. For this demand, we design a specimen slicer for domain users to navigate the data and select slices with proper thickness. As shown in Fig. 7, users can fix a clipping orientation by rotating the box in the orthogonal view. The posture of the box will be automatically aligned to axis if it is close to axis directions. Then the two clipping planes for slicing can be assigned by moving the callipers on the left side. This user interface is helpful for selecting meaningful sections of the volume data.

6.2 Focus+Context Lenses

In our system, we also provide focus+context lenses to illustrate the results. It often occurs that one image generated by single rendering method cannot reveal all aspects of the features. Inspired by VolumeShop [3], we enable users to select a region on the image space to visualize the data with selected microscopy techniques. In practical, this function is very useful since several techniques can be simultaneously applied on the same data. As shown in Fig. 8, DVR can present a good overview on the outline and shape of the data, and the microscopy volume visualization can better enhance the detailed features on top of the context of DVR.

6.3 Multi-Wavelength Interference Microscopy Volume Illustration

In some cases, only one fixed wavelength is not enough to present multiple features that are interested. In our tool, users can select a few locations on the display and specify the proper corresponding frequency values to emphasize different features. The wavelength λ then can be interpolated through out the whole image by GPU and saved into an intermediate texture. A texture lookup for wavelength λ is then employed to compute each pixel's intensity after interference interaction. We call this approach as phase-contrast Volume Rendering with Multi-wavelength (PCVR(MW)) in contrast to the previously mentioned single wavelength method. As illustrated in Fig. 9, user can define control points on the screen as shown in Fig. 9(b). Each control point represents a wave length value λ_i .

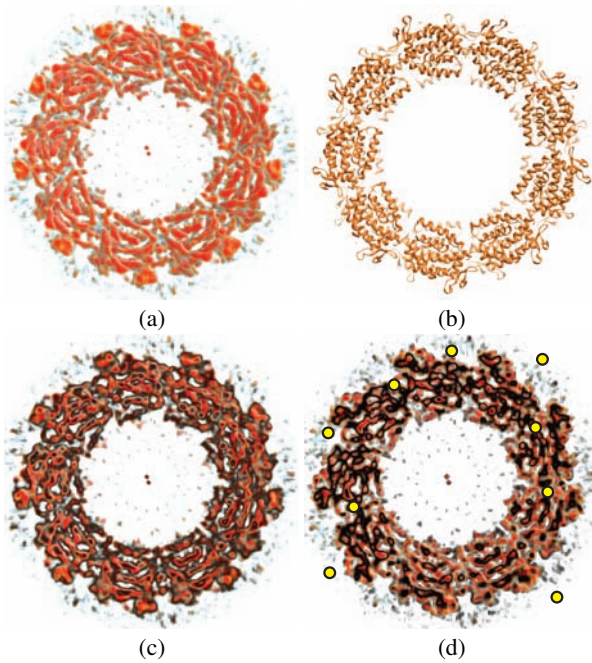


Figure 9: PCVR with multiple wavelength modulated: (a) DVR image; (b) The actual crystal structure of the data; (c) PCVR with unique wavelength; (d) PCVR with multiple different wavelengths. The yellow points in (c) are control points defining different wavelengths.

The wave lengths of non-defined region can be achieved by smooth interpolation:

$$l(\mathbf{x}) = \sum_i \omega_i \lambda_i, \quad (18)$$

where weights ω are defined as the transformation of the distances to the control points:

$$\omega_i = \frac{1/(1+d(x-x_i))}{\sum_i 1/(1+d(x-x_i))}. \quad (19)$$

7 RESULTS AND PERFORMANCE

We have applied our methods on three biomedical datasets, including mouse intestine microvilli data, rATCpnbeta Cryo-EM reconstruction data, and neuron tomogram data of the *C.elegans* neuron synapse. The data specifications are enumerated in Table 1.

7.1 Mouse Intestine Microvilli Data

As shown in Fig. 1, the mouse intestine microvilli data set is visualized with lens of PCVR and DICVR in the context of background image rendered with DVR.

In this case, domain scientists mainly focus on three types of structures, including the capping proteins, the membranes, as well as the micro-filament matters inside the cells. The first two features can be identified with traditional DVR through 1D TF design. However, the micro-filament structures are very hard to be distinguished from the surrounding matters using traditional methods. As seen in the DICVR lens, micro-filament and thread like features can be clearly illustrated. With PCVR lens, the structures with abrupt density variation are enhanced. This case clearly demonstrate the advantages of our proposed techniques over existing volume rendering.

7.2 rATCpnbeta Data

The group II chaperonin rATCpnbeta data [11], which is from Cryo-EM single particle reconstruction, is reconstructed at the the resolution of 8.4Å. It is a chaperone with a axis-based five-folded symmetry structure. It is challenging to directly visualize the reconstructed

Dataset	Resolution	DVR	PCVR	PCVR _M	DICVR	DICVR _M
Microvilli	1747 × 1742 × 221	273.2	584.1	590.0	380.3	388.9
rATCpnbeta	160 ³	28.7	35.2	38.3	38.4	43.6
Neuron Synapse	512 ² × 192	85.3	117.1	119.0	125.4	128.4

Table 1: The average timings (in milliseconds) of our rendering method with various models, including DVR, PCVR, multi-wavelength PCVR, DICVR and multi-wavelength DICVR respectively.

volume data for reasons. The noise of the data is often very high, so meaningful features are not easy to be classified by TFs. The contrast of the rendered image is not ideal with traditional methods since the structures belonging to the same feature is overlapped and folded (Fig. 9(a), (b)). On the other hand, analyzing data on such scale of wavelength is not available with real world microscopy. Users can use existing microscopy metaphor and analytics methods to investigate such volume data with our tool.

We have generated a group of visualization results for this data, with different methods and wavelengths (Fig. 10). With shorter wavelength, detailed structures can be enhanced but artifacts may increase due to the noise. The initial phase, which corresponds to the phase plate in real microscopes, can regulate the contrast of the image.

7.3 Electron Tomogram Data of the *C.elegans* Neuron Synapse

In Fig. 11, we demonstrate the rendering results of tomogram data of the *C.elegans* neuron synapse [23] with our methods. The TF for DVR is quite tricky to design because the distribution of features is very concentrated to a small numerical range with high noise. The result of DVR is occluded and noisy. By utilizing PCVR, the contrast of inner structures are enhanced and visualized, although there are a few artifacts in boundary areas. Especially, the nucleus and the membranes are highlighted. In the DICVR result, the contrast is further enhanced, and the image brings strong stereoscopic impression. The boundary of the features look like the valleys in the image. In the neuron synapse data, one of the most important features to be identified is the microtubules. The location of microtubules are much easier to be identified in both the rendering results of DICVR and PCVR than that of DVR. As illustrated in

As the proposed methods are originated from biology and microscopy science and technology, it is very straightforward for domain users to comprehend and use. Although the standard DVR can indeed help on data comprehension, the TF design for such data is very difficult for domain users. The proposed methods are strong complements to existing technologies.

7.4 Performance

The system is implemented in C++ and GLSL shading language. We leverage the current commodity graphics hardware to perform the computing and rendering. Table 1 shows the timing for the rendering of different datasets. For each data set, we measure the rendering time of DVR, PCVR, and DICVR. For PCVR and DICVR, we also measure the performance of multi-wavelength rendering. All experiments have been performed on a Dell Precision T3500 workstation with a Intel Xeon 2.40G Hz CPU, 8GB RAM, and an NVidia GTX 470 graphics card with 1280MB video memory. All images are generated at a screen resolution of 640 × 480 pixels. The raycasting step size is fixed at 1 voxel. All data that are tested are with 32-bit float precision.

As shown in the table, the performance of both PCVR and DICVR are only slightly lower than DVR. Besides, the performance difference between the single wavelength and multi-wavelength is almost the same. In multi-wavelength mode, the wavelength interpolation process is all computed by GPU and only need to be done once for each rendering. The main performance difference is due to texture lookup for the wavelength of each pixel.

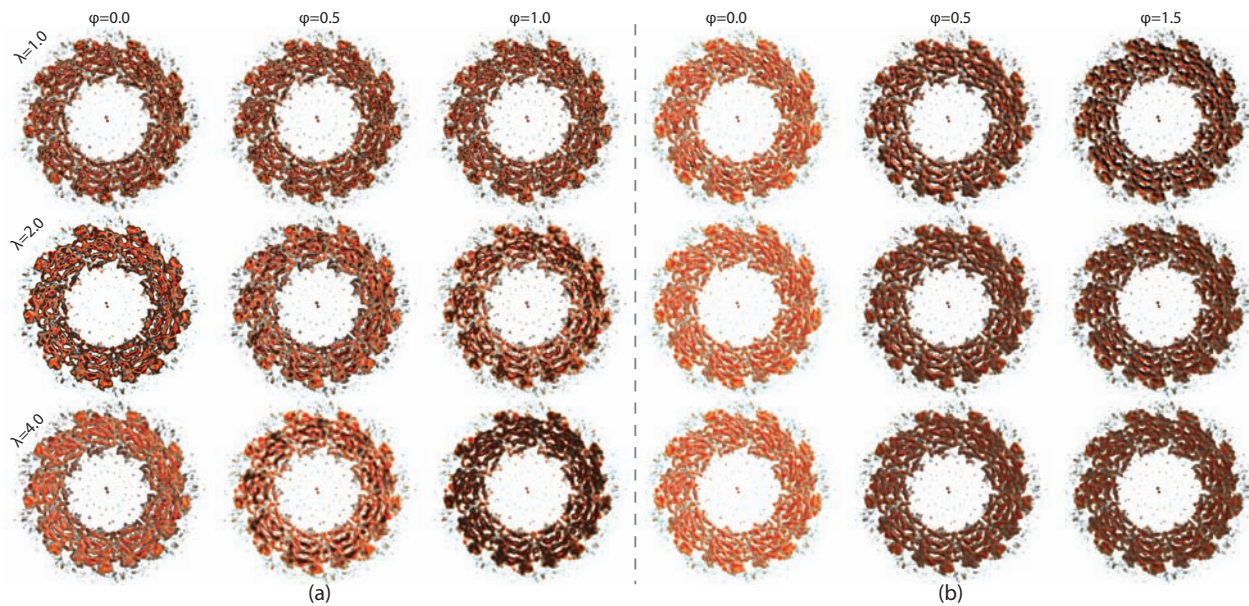


Figure 10: The interference microscopy volume rendering of rATCpnbeta data with PCVR (a) and DICVR (b) in different wavelengths and phase. The DVR image is shown in Fig. 9(a).

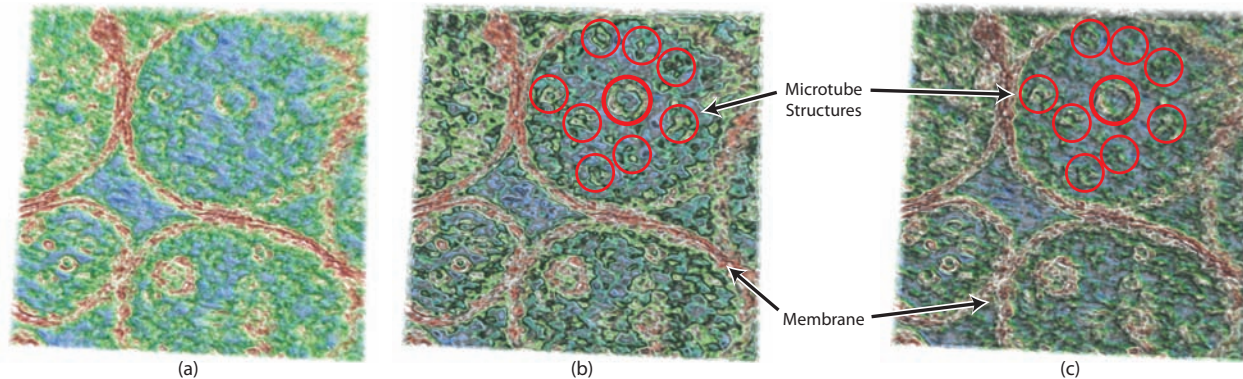


Figure 11: Visualization results for electron tomogram of neuron synapse data with different methods. Structures of microtubules are much easier to be identified with methods we proposed: (a) DVR. The features are severely submerged with the surroundings; (b) PCVR. The contrast of the image is enhanced. The outlines of inner features appear; (c) DICVR. The contrast of the image is enhanced by introducing emboss effects that are brought by DICVR. Inner structures are clearly visualized.

8 DISCUSSION AND DOMAIN EXPERTS' FEEDBACK

The aforementioned volume visualization results are generated and tuned as joint efforts from both visualization experts and domain scientists. In our experiments, domain scientists, mostly from biophysics research including one co-author of this paper, tried the visualization system we implemented and gave very positive feedbacks. The scientists considered both PCVR and DICVR can be utilized as complementary tools of DVR for data visualization and very useful in many difficult visualization cases.

First of all, our techniques of DICVR and PCVR provide compatible rendering results to real microscopy images which is not possible to be achieved through transfer function specification in traditional volume rendering. As modern tomogram and scanning techniques can obtain the density value at each sample point, it is desirable to establish compatible approaches to relate the data with traditional observational results from optical methods. Domain scientists received vigorous training on using microscopy techniques. They are much more familiar with and sensitive to the style our approaches can provide. Generation of microscopy-like images with similar underlying physical principles could enable the cross-comparison between results from different acquisition sources.

Furthermore, domain scientists appreciated our approaches on

providing imagery results with strongly enhanced details. The difference is very apparent in the case of visualizing the mouse intestine microvilli data set using DICVR (Fig. 1). One co-author of this paper used commercial visualization software such as Amira and a few other advanced volume illustration systems to render the data before. Due to the noisy nature of the microvilli data, previous approaches are not able to clearly identify the small micro-filament structures embedded in each microvillus even with carefully tuned transfer functions. Our proposed visualization techniques provides results with clear illustration of the structures. This capability is strongly recommended by the domain scientists. Domain scientists also suggest that our methods have potential to better depict surfaces with small variation in the scale compatible to the wavelength employed, as similar applications are common for light interference. Although we haven't test in this direction at this stage, in the future, we would like to include data with aforementioned properties in our research to further explore the potential of our approaches.

Both the interaction methods of focus+context lens and slicing have been considered as very useful by the domain users, although they are relatively simple from the view of visualization experts. In biomedical study, most real acquired data sets are very noisy. Ren-

dering thick layers of volume may mix too much noise and overwhelm the desirable fine structures. Interactive selection of layer thickness and convenient panning the layer window enable flexible exploration of the data and help to discover structures inside the data. The lens can further make the comparison between different rendering styles simple.

We also notice the limitations of our methods. Unwanted strips may appear in the visualization results due to the mismatched parameter configuration or the thickness of the specimen. The strips, however, can also be used as the indication of the thickness variation. Balanced results could be achieved by proper wavelength setting or using focus+context lens with the DVR background.

9 CONCLUSION AND FUTURE WORK

In this paper, we present novel visualization methods for illustrating volumetric data inspired by interference microscopies, including both phase-contrast and DIC microscopy. Our proposed methods provides compatible rendering results to real microscopy images which are easier to be comprehended by domain users. Our results show that the methods are capable of illustrating and enhancing the inner detailed structures in noisy data sets. Our work provides a new way of visualize volume data capturing special lighting effects of interferences. By further leveraging commodity graphics hardware, user interface with lens and slicing capabilities implemented provides interactivities of the system.

One major future improvement is the selection of parameters. Currently, the wavelengths and phases are interactively assigned by users. In the future, we plan to further improve the usability of our work by designing better ways of defining parameters in our proposed visualization methods. Automatic mechanisms could be employed to set good initial parameters. In addition, the manual tuning is still useful because users can be conscious about the thickness variation of the data during the tuning process.

ACKNOWLEDGEMENTS

The authors wish to thank the anonymous reviewers for their insightful comments. We are grateful to Prof. Jean-Louis Bessereau (IBENS, France) for his kindness of sharing the tomography data of *C.elegans* neuron cell section. This work is supported by National Natural Science Foundation of China Project No. 60903062 and 61170204, Beijing Natural Science Foundation Project No. 4092021, 863 Program Project 2010AA012400, Chinese Ministry of Education Key Project No. 109001, and Chinese Academy of Sciences (KGCX1-YW-13).

REFERENCES

- [1] B. Böttcher, S. A. Wynne, and R. A. Crowther. Determination of the fold of the core protein of hepatitis b virus by electron cryomicroscopy. *Nature*, 386:88–91, 1997.
- [2] C. Brownlee, V. Pegoraro, S. Shankar, P. McCormick, and C. D. Hansen. Physically-based interactive flow visualization based on schlieren and interferometry experimental techniques. *IEEE Trans. Vis. Comput. Graph.*, 17(11):1574–1586, 2011.
- [3] S. Bruckner and M. E. Gröller. VolumeShop: An interactive system for direct volume illustration. In *Proceedings of IEEE Visualization 2005*, pages 671–678, 2005.
- [4] S. Bruckner and M. E. Gröller. Enhancing depth-perception with flexible volumetric halos. *IEEE Trans. Vis. Comput. Graph.*, 13(6):1344–1351, 2007.
- [5] B. Csébfalvi, L. Mroz, H. Hauser, A. König, and E. Gröller. Fast visualization of object contours by non-photorealistic volume rendering. *Comput. Graph. Forum*, 20(3):452–460, 2001.
- [6] M. Dias. Ray tracing interference color. *IEEE Comput. Graph. Appl.*, 11(2):54–60, 1991.
- [7] F. Dong, G. J. Clapworthy, H. Lin, and M. A. Krokos. Nonphotorealistic rendering of medical volume data. *IEEE Comput. Graph. Appl.*, 23(4):44–52, 2003.

- [8] D. Ebert and P. Rheingans. Volume illustration: Non-photorealistic rendering of volume models. In *Proceedings of IEEE Visualization 2000*, pages 195–202, 2000.
- [9] K. Engel, M. Hadwiger, J. M. Kniss, C. Rezk-Salama, and D. Weiskopf. *Real-Time Volume Graphics*. A. K. Peters, 2006.
- [10] J. S. Gondek, G. W. Meyer, and J. G. Newman. Wavelength dependent reflectance functions. In *Proceedings of SIGGRAPH 1994*, pages 213–220, 1994.
- [11] Y. Huo, Z. Hu, K. Zhang, L. Wang, Y. Zhai, Q. Zhou, G. Lander, J. Zhu, Y. He, X. Pang, W. Xu, M. Bartlam, Z. Dong, and F. Sun. Crystal structure of group II chaperonin in the open state. *Structure*, 18:1270–1279, 2010.
- [12] V. Interrante, H. Fuchs, and S. Pizer. Enhancing transparent skin surfaces with ridge and valley lines. In *Proceedings of IEEE Visualization 1995*, pages 52–59, 1995.
- [13] J. Kniss, G. Kindlmann, and C. Hansen. Interactive volume rendering using multi-dimensional transfer functions and direct manipulation widgets. In *Proceedings of IEEE Visualization 2001*, pages 255–262, 2001.
- [14] J. Kniss, G. Kindlmann, and C. Hansen. Multidimensional transfer functions for interactive volume rendering. *IEEE Trans. Vis. Comput. Graph.*, 8(3):270–285, 2002.
- [15] J. Kruger and R. Westermann. Acceleration techniques for GPU-based volume rendering. In *Proceedings of IEEE Visualization 2003*, pages 38–45, 2003.
- [16] M. Levoy. Display of surfaces from volume data. *IEEE Comput. Graph. Appl.*, 8(3):29–37, 1988.
- [17] A. Lu, C. Morris, J. Taylor, D. S. Ebert, C. Hansen, P. Rheingans, and M. Hartner. Illustrative interactive stipple rendering. *IEEE Trans. Vis. Comput. Graph.*, 9(2):127–138, 2003.
- [18] A. Lu, C. J. Morris, D. S. Ebert, P. Rheingans, and C. Hansen. Non-photorealistic volume rendering using stippling techniques. In *Proceedings of IEEE Visualization 2002*, pages 211–218, 2002.
- [19] T. Luft, C. Colditz, and O. Deussen. Image enhancement by unsharp masking the depth buffer. *ACM Trans. Graph.*, 25(3):1206–1213, 2006.
- [20] H. Pfister, W. E. Lorensen, C. L. Bajaj, G. L. Kindlmann, W. J. Schroeder, L. S. Avila, K. Martin, R. Machiraju, and J. Lee. The transfer function bake-off. *IEEE Comput. Graph. Appl.*, 21(3):16–22, 2001.
- [21] S. Roettger, S. Guthe, D. Weiskopf, T. Ertl, and W. Strasser. Smart hardware-accelerated volume rendering. In *VisSym '03: Proceedings of the symposium on Data visualisation 2003*, pages 231–238, 2003.
- [22] S. Stegmaier, M. Strengert, T. Klein, and T. Ertl. A simple and flexible volume rendering framework for graphics-hardware-based raycasting. In *Proceedings of Eurographics / IEEE VGTC Workshop on Volume Graphics 2005*, pages 187–195, 2005.
- [23] C. Stigloher, H. Zhan, M. Zhen, J. Richmond, and J.-L. Bessereau. The presynaptic dense projection of the caenorhabditis elegans cholinergic neuromuscular junction localizes synaptic vesicles at the active zone through SYD-2/Liprin and UNC-10/RIM-dependent interactions. *The Journal of Neuroscience*, 31(12):4388–4396, 2011.
- [24] Y. Sun, F. D. Fracchia, T. W. Calvert, and M. S. Drew. Deriving spectra from colors and rendering light interference. *IEEE Comput. Graph. Appl.*, 19(4):61–67, 1999.
- [25] N. Svakhine and D. S. Ebert. Interactive volume illustration and feature halos. In *Proceedings of Pacific Graphics 2003*, pages 347–354, 2003.
- [26] N. Svakhine, D. S. Ebert, and D. Stedney. Illustration motifs for effective medical volume illustration. *IEEE Comput. Graph. Appl.*, 25(3):31–39, 2005.
- [27] N. Svakhine, Y. Jang, D. S. Ebert, and K. P. Gaither. Illustration and photography inspired visualization of flows and volumes. In *Proceedings of IEEE Visualization 2005*, page 87, 2005.
- [28] S. Treavett and M. Chen. Pen-and-ink rendering in volume visualization. In *Proceedings of IEEE Visualization 2000*, pages 203–210, 2000.
- [29] X. Yuan and B. Chen. Illustrating surfaces in volume. In *VisSym'04: Proceedings of Joint IEEE/EG Symposium on Visualization*, pages 9–16, 2004.